ROCK1 but not ROCK2 contributes to RhoA signaling and NMIIA-mediated contractility at the epithelial zonula adherens

Rashmi Priya*,†, Xuan Liang, Jessica L. Teo, Kinga Duszyc, Alpha S. Yap, and Guillermo A. Gomez*
Division of Cell Biology and Molecular Medicine, Institute for Molecular Bioscience, University of Queensland, St. Lucia, Brisbane, QLD 4072, Australia

ABSTRACT **Rho kinases (ROCK1 and ROCK2) function downstream of the small GTPase RhoA to drive actomyosin cytoskeletal remodeling. It has often been believed that ROCK1 and ROCK2 may be functionally redundant, as they share a highly conserved kinase domain. However, in this study, we report differential functional effects for these ROCKs at the epithelial zonula adherens (ZA). Using specific siRNA, we found that ROCK1 depletion disrupted cadherin organization at the ZA, accompanied by loss of F-actin and NMIIA, whereas ROCK2 knockdown had no significant effect. Further, ROCK1, but not ROCK2, was necessary to stabilize GTP-RhoA at the ZA, thereby sustaining junctional tension and inhibiting intraepithelial cell movement. We also found that nonmuscle myosin IIA is a major determinant of ROCK1 cortical stability. Thus, despite sharing the catalytic domain with ROCK2, ROCK1 appears to be the dominant kinase essential for junctional integrity and contractile tension at epithelial ZA.**

Monitoring Editor
Jeffrey D. Hardin
University of Wisconsin

Received: Apr 29, 2016
Revised: Oct 7, 2016
Accepted: Oct 26, 2016

INTRODUCTION

Rho-dependent kinases (ROCKs) are major regulators of the actomyosin cytoskeleton and thus govern a variety of cellular processes, including cell division, migration, polarity, and epithelial homeostasis (Bishop and Hall, 2000; Riento and Ridley, 2003). They belong to the family of Ser/Thr kinases, and two proteins have been reported in mammalian cells: ROCK1 and ROCK2 (Nakagawa *et al.*, 1996). Broadly, these proteins are constitutive dimers, each subunit containing an N-terminal kinase domain followed by a coiled-coil domain and a C-terminus that contains a canonical Rho-binding domain (RBD) and a pleckstrin homology (PH) domain (Jacobs *et al.*, 2006; Garg *et al.*, 2008; Truebestein *et al.*, 2015). Overall they share 62% identity, with the kinase domain being highly conserved (92% identity) and the coiled-coil domain being the most divergent (55% identity; Amano *et al.*, 2010; Julian and Olson, 2014). Two different modes for ROCK activation have been described. One widely accepted model suggests that the C-terminus of ROCK binds to the N-terminus, leading to inhibition of ROCK activity. Association of GTP-Rho to the RBD releases this autoinhibitory conformation to activate the kinase (Amano *et al.*, 1996; Matsui *et al.*, 1996). In the second mode of activation, particularly relevant for ROCK2, Rho signaling is not necessary for ROCK2 activation, and instead the length of its coiled-coil domain is a key determinant of its kinase activity (Truebestein *et al.*, 2015).

Because the two ROCK proteins share a highly conserved kinase domain, it has been postulated that they may perform similar biological functions by phosphorylating common substrates. Indeed, using conditional knockout mice, it has been reported that ROCK1 and ROCK2 act redundantly to modulate MYPT phosphorylation and actomyosin contractility (Kumper *et al.*, 2016). However, there are various reports suggesting that ROCK proteins exhibit distinct functions and regulation. In the context of cell–matrix adhesion, ROCK1 was required for the maturation of focal adhesion complexes and stress fiber formation, whereas ROCK2 knockdown enhanced the formation of stress fibers and focal adhesions (Yoneda *et al.*, 2005; Lock *et al.*, 2012). In fibroblasts, depletion of ROCK2 led to a clearly defined front and rear polarity, whereas ROCK1 knockdown resulted in a complete loss of polarity

This article was published online ahead of print in MBoC in Press (http://www.molbiolcell.org/cgi/doi/10.1091/mbc.E16-04-0262) on November 9, 2016.

†Present address: Department of Developmental Genetics, Max Planck Institute for Heart and Lung Research, 61231 Bad Nauheim, Germany.

*Address correspondence to: Rashmi Priya (rashmi.priya@mpi-bn.mpg.de), Guillermo A. Gomez (g.gomez@uq.edu.au).

Abbreviations used: MRLC, myosin regulatory light chain; NMII, nonmuscle myosin II; NMIIA, nonmuscle myosin II A; NMIIB, nonmuscle myosin II B; pMRLC, phosphorylated myosin regulatory light chain; ROCK, Rho-dependent kinase; ZA, zonula adherens.

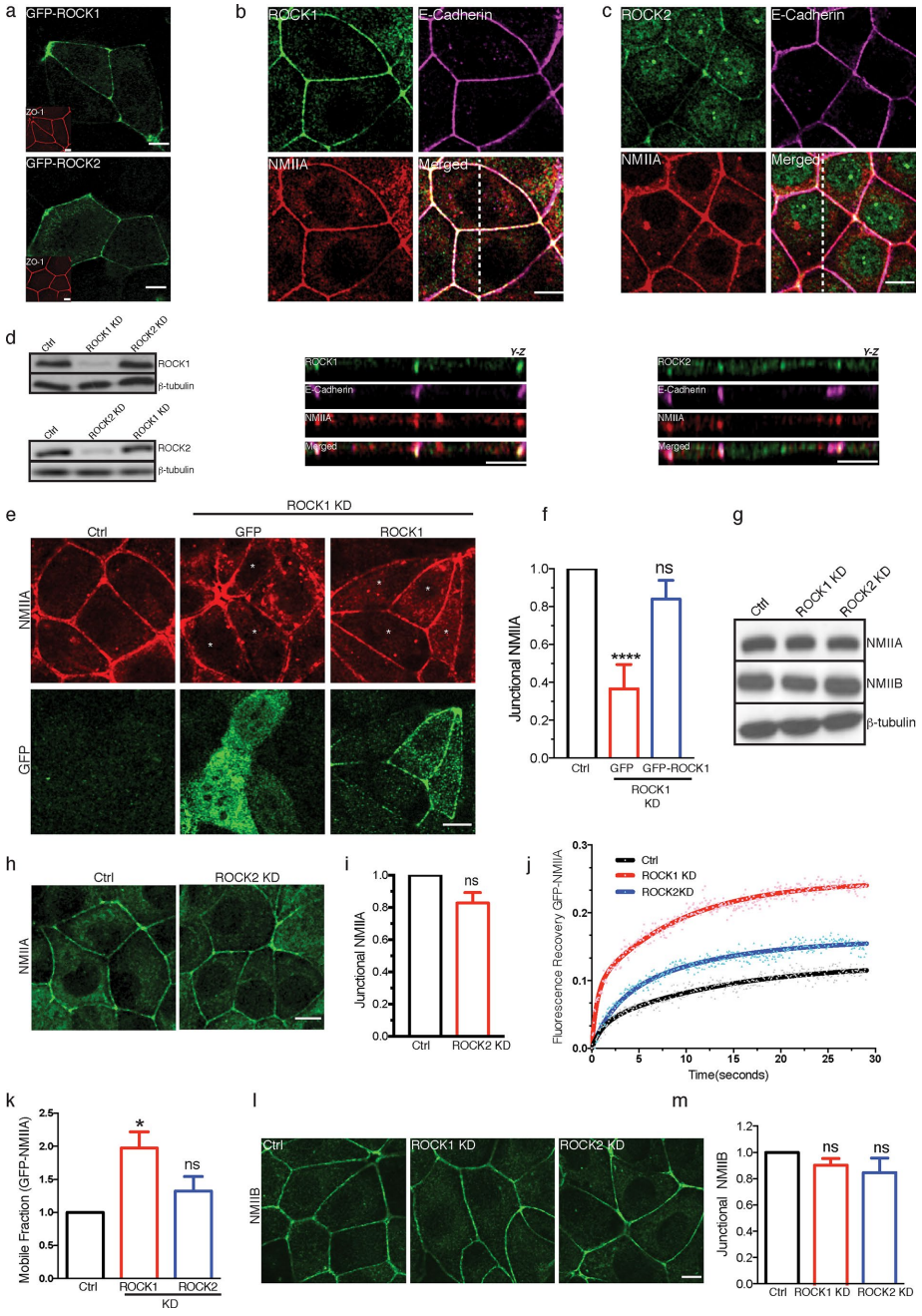

FIGURE 1: ROCK1 depletion affects NMIIA localization and stability. (a) GFP-ROCK1/ROCK2 localization in MCF-7 cells. (b, c) Endogenous ROCK1/ROCK2 localization in MCF-7 cells; *yz* images indicate the apical concentration of ROCKs with NMIIA and E-cadherin. (d) ROCK1, ROCK2, and β-tubulin immunoblots from the Ctrl, ROCK1 KD, or ROCK2 KD MCF-7 cell lysates. (e, f) NMIIA localization in Ctrl, ROCK1 KD, and ROCK1 KD + GFP ROCK1 cells and the corresponding line-scan analysis ($n = 3$). (g) NMIIA, NMIIB, and β-tubulin immunoblots from the Ctrl, ROCK1 KD, or ROCK2 KD MCF-7 cell lysates. (h, i) NMIIA localization in Ctrl and ROCK2 KD cells and the corresponding line-scan analysis ($n = 3$). (j, k) FRAP of apical GFP-NMIIA in Ctrl, ROCK1 KD, and ROCK2 KD MCF-7 cells; mobile fraction values were calculated in GraphPad Prism ($n = 3$). (l, m) NMIIB localization in Ctrl, ROCK1 KD, and ROCK2 KD cells and the corresponding line-scan analysis ($n = 3$).

and perturbation of peripheral actomyosin networks (Newell-Litwa *et al.*, 2015). Further, ROCK1 has been shown to specifically interact with and phosphorylate Rnd3 (Riento *et al.*, 2005; Komander *et al.*, 2008) and interact with p120-catenin (Smith *et al.*, 2012) and formin FHOD1 (Hannemann *et al.*, 2008), whereas MYPT-1 interacts with ROCK-2 but not ROCK1 (Wang *et al.*, 2009).

ROCK is an important regulator of cadherin organization and function in cell–cell adhesion. ROCK inhibition perturbed apical F-actin and E-cadherin organization and disrupted epithelial adherens junction assembly in a calcium-switch assay (Anderson *et al.*, 2002; Smith *et al.*, 2012; Andreeva *et al.*, 2014). One of the principal downstream effectors of ROCK at adherens junctions is nonmuscle myosin II (NMII; Shewan *et al.*, 2005). ROCK activates NMII by phosphorylating the Ser-19/Thr-18 residues of the NMII regulatory light chain (MRLC) and also by inhibiting the MRLC phosphatase MYPT-1 (Amano *et al.*, 1996; Kimura *et al.*, 1996). This stimulates the ATPase activity of NMII, leading to generation of contractile forces and stability of cadherin junctions (Ratheesh *et al.*, 2012; Priya and Gomez, 2013; Priya *et al.*, 2015; Wu *et al.*, 2014). Further, ROCK was recently found to participate in a feedback network that supported RhoA signaling at cadherin junctions (Priya *et al.*, 2015, 2016). However, distinct contributions of ROCK1 and ROCK2 to junctional biology have yet to be investigated in detail. Accordingly, in the present study, we sought to dissect the selective functions of ROCKs at epithelial cadherin junctions. Our data demonstrate that ROCK1, but not ROCK2, is required for zonula adherens (ZA) organization, RhoA signaling, and cortical tension, which in turn restricts epithelial motility. Of interest, ROCK1 selectively supports nonmuscle myosin IIA (NMIIA) localization at the ZA, which in turn acts as a principal regulator of ROCK1 stability.

RESULTS AND DISCUSSION

ROCK1, but not ROCK2, determines cortical myosin II localization and stability

We began by characterizing the localization of ROCK proteins at the ZA in MCF-7 and Caco-2 epithelial cells. Green fluorescent protein (GFP)–tagged transgenes of ROCK1 and ROCK2 concentrated at the apical junctions as marked by ZO-1 (Figure 1a). Further, both proteins were detected in cell lysates (Figure 1d and Supplemental Figure S1d), and immunofluorescence revealed that endogenous ROCK1 and ROCK2 were enriched at the ZA in both cell lines (Figure 1, b and c, and Supplemental Figure S1, a–c).

To gain insight into the potential effect of individual ROCKs on the ZA, we examined how ROCK depletion affected the cortical pool of phosphorylated myosin regulatory light chain (pMRLC) and NMII, as these are canonical effectors of the RhoA-ROCK pathway that support junctional contractility and integrity

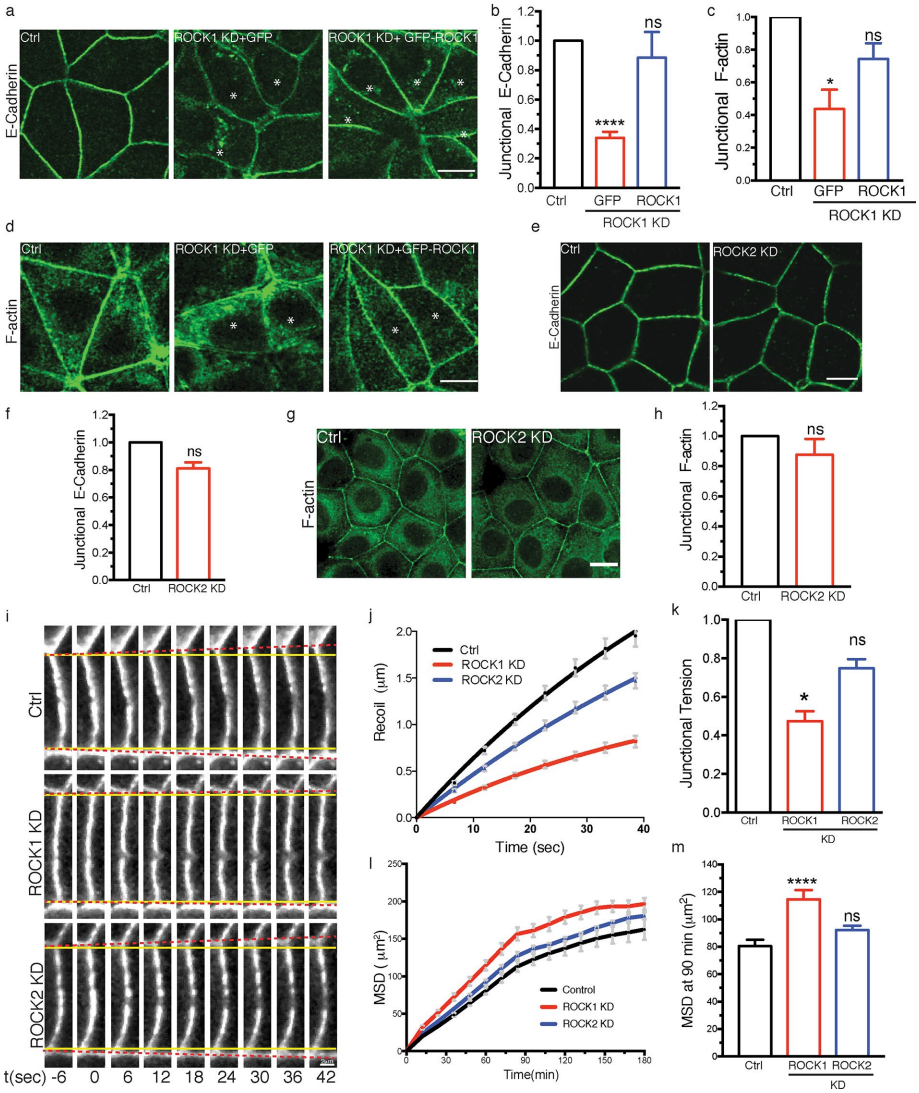

FIGURE 2: ROCK1 supports ZA organization and junctional tension and restricts epithelial motility. (a, b) E-cadherin localization in Ctrl, ROCK1 KD, and ROCK1 KD + GFP-ROCK1 MCF-7 cells and the corresponding line-scan analysis ($n = 3$). (c, d) F-actin localization in Ctrl, ROCK1 KD, and ROCK1 KD + GFP-ROCK1 MCF-7 cells and the corresponding line-scan analysis ($n = 3$). (e–h) E-cadherin and F-actin localization in Ctrl and ROCK2 KD MCF-7 cells and the corresponding line-scan analysis ($n = 3$). (i) Representative confocal images at different time points before and after nanoablation performed with E-cadherin-GFP–expressing MCF-7 cells transfected with control or ROCK1 or ROCK2 siRNA. Scale bar, 2 μm. Yellow line indicates the initial position, and red dashed line indicates the displaced junctions after ablation. (j, k) Best-fit single-exponential curves and tension (initial recoil) derived from nanoablation experiments ($n = 3$). (l, m) Time course (l) and average (at 90 min) mean square displacement (MSD) of the moving nuclei in MCF-7 control, ROCK1 KD, and ROCK2 KD confluent monolayers. Plots are average from five different fields, and 750–1000 nuclear tracks per field were analyzed.

(Shewan *et al.*, 2005; Smutny *et al.*, 2010; Ratheesh *et al.*, 2012; Priya *et al.*, 2013; Wu *et al.*, 2014). Inhibition of ROCK by Y-27632 and ROCK1 knockdown (KD) significantly reduced pMRLC content at the ZA in MCF-7 cells (Supplemental Figure S1, e and f). Moreover, junctional NMIIA localization (but not its overall expression level) was significantly reduced by ROCK1 KD in both MCF-7 (Figure 1, e–g,) and Caco-2 (Supplemental Figure S1, g–i) cells, a phenotype that was rescued by expression of an RNA interference (RNAi)–resistant ROCK1 transgene (Figure 1, e and f), confirming the specificity of these effects. In contrast, ROCK2 KD had no significant effect on junctional pMRLC and NMIIA in either cell line (Figure 1, h and i, and Supplemental Figure S1, g and h). To further pursue this, we analyzed the effect of ROCK knockdown on the junctional dynamics of NMIIA using fluorescence recovery after photobleaching (FRAP). ROCK1, but not ROCK2, depletion led to a significant increase in the mobile fraction of the apical pool of NMIIA, confirming that ROCK1 was selectively required to stabilize NMIIA at ZA (Figure 1, j and k).

Of note, junctional NMIIB content was unaffected by depletion of either ROCK1 or ROCK2, both in MCF-7 (Figure 1, l and m) and Caco-2 cells (Supplemental Figure S1, j and k). Because both myosin paralogues have a similar RLC, this raises the question of how ROCK1 can selectively support the junctional localization of NMIIA. One possibility is that this reflects the higher expression of NMIIA than NMIIB in MCF-7 cells (Smutny *et al.*, 2010). Further, our recent finding that ROCK1 can selectively immunoprecipitate NMIIA (Priya *et al.*, 2015) raises the possibility that ROCK1 might interact more strongly with NMIIA than with NMIIB. By whatever mechanism(s), the apparently dominant effect of ROCK1 on NMIIA localization supports earlier evidence that the junctional localizations of NMIIA and NMIIB are subject to different upstream signals, with the RhoA-ROCK pathway being the key determinant of NMIIA localization (Sandquist *et al.*, 2006; Smutny *et al.*, 2010; Gomez *et al.*, 2015).

ROCK1 regulates ZA organization to support junctional tension and restricts epithelial motility

Because NMIIA is a key determinant of ZA integrity and contractility (Ratheesh *et al.*, 2012; Priya *et al.*, 2013), we then asked how ROCK1 might affect these properties of the junction. Compared with control cells, E-cadherin and F-actin failed to concentrate into tight, ring-like structures at the apical junctions in ROCK1 KD cells, and this could be restored by RNAi-resistant full-length ROCK1 (Figure 2, a–d, and Supplemental Figure S2, a–d). Quantification revealed a significant decrease in the fluorescence intensity of E-cadherin and F-actin, although protein expression and cell density were unchanged (Figure 2, a–d, and Supplemental Figure S2, a–g). Further, tight junction integrity, as reflected by ZO-1 staining, was not overtly compromised, suggesting a selective effect on ZA (Supplemental Figure S2h). ROCK2 depletion did not affect either E-cadherin or F-actin, consistent with the dominant effect of ROCK1 that we observed for NMIIA (Figure 2, e–h, and Supplemental Figure S2, a–d).

The reduction of E-cadherin, F-actin, and NMIIA at the ZA led us to predict that ROCK1 depletion would also affect junctional contractility. To test this, we cut the apical junctions (marked by expression of E-cadherin–GFP) using a femtosecond pulsed

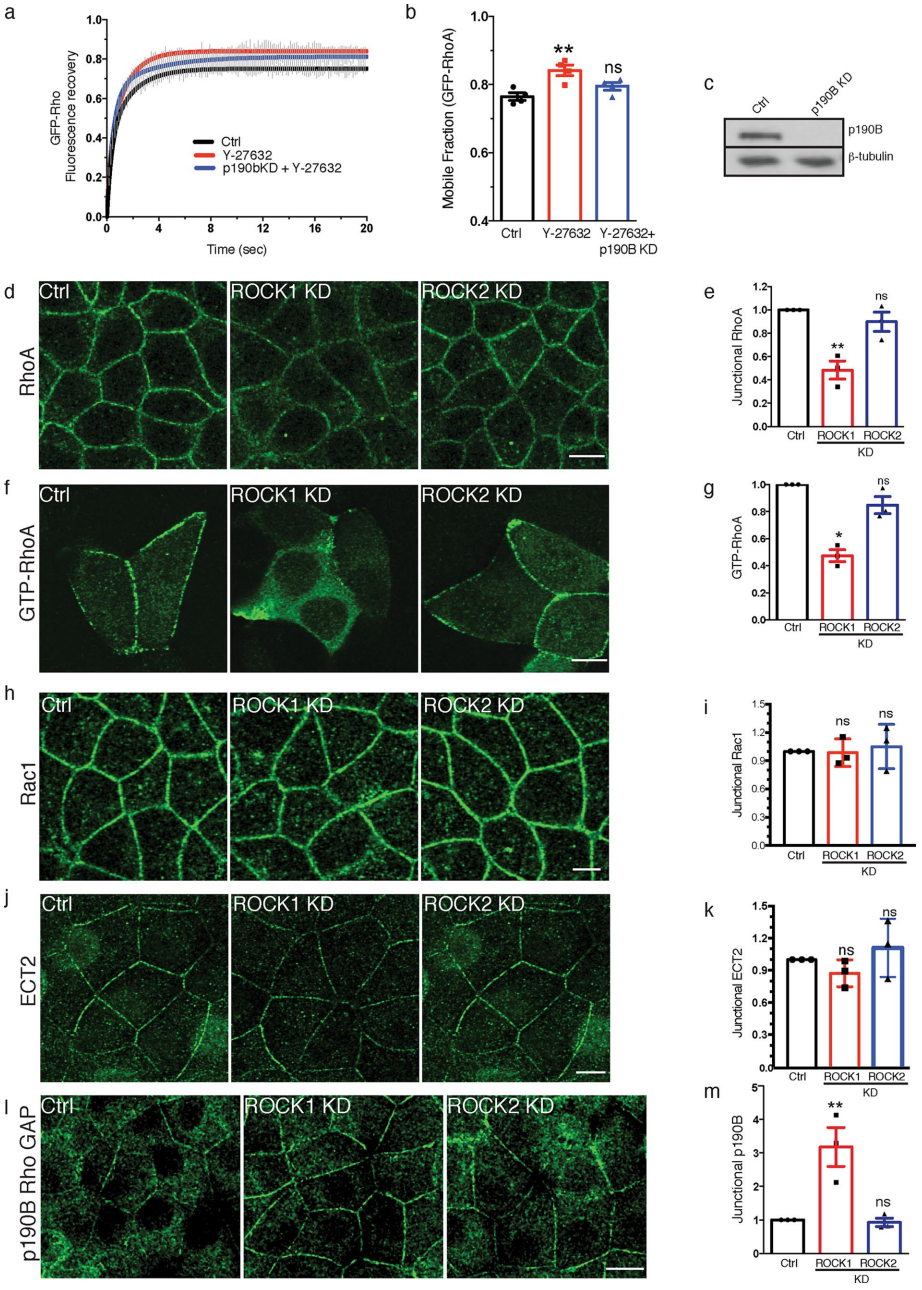

FIGURE 3: ROCK1 supports Rho signaling at the ZA. (a, b) FRAP of junctional GFP-RhoA in Ctrl or p190B KD MCF-7 cells treated with either PBS or Y-27632. Mobile fraction values were calculated by fitting the recovery curves to a biexponential function in GraphPad Prism ($n = 4$). (c) Lysates from Ctrl and p190B KD MCF-7 cells immunoblotted for p190B Rho GAP and β-tubulin. (d, e) RhoA localization in Ctrl, ROCK1 KD, and ROCK2 KD MCF-7 cells and the corresponding line-scan analysis ($n = 3$). (f, g) GFP-AHPH (GTP-RhoA) localization in Ctrl, ROCK1 KD, and ROCK2 KD MCF-7 cells and the corresponding line-scan analysis ($n = 3$). (h, i) Rac1 localization in Ctrl, ROCK1 KD, and ROCK2 KD MCF-7 cells and the corresponding line-scan analysis ($n = 3$). (j, k) ECT2 localization in Ctrl, ROCK1 KD, and ROCK2 KD MCF-7 cells and the corresponding line-scan analysis ($n = 3$). (l, m) p190B GAP localization in Ctrl, ROCK1 KD, and ROCK2 KD MCF-7 cells and the corresponding line-scan analysis ($n = 3$).

laser and measured the speed of the initial recoil of the vertices as an index of the preexisting tension (Ratheesh *et al.*, 2012). Depletion of ROCK1, but not ROCK2, caused a significant reduction in the initial recoil velocity without affecting apparent junctional viscous drag (Figure 2, i–k; see *Materials and Methods*), reinforcing the notion that ROCK1 supports cortical tension at the ZA by promoting NMIIA-mediated contractility.

Finally, we asked what functional effect might arise from the ability of ROCK1, but not ROCK2, to regulate junctional tension. For this, we focused on epithelial motility and assessed the role of ROCK proteins on the movement of MCF-7 cells grown as confluent monolayers. Using particle-tracking software to quantitate the movement of nuclei (Jaqaman *et al.*, 2008; Ng *et al.*, 2012), we found that control cells showed low levels of locomotility (measured as mean squared displacement; Figure 2, l and m, and Supplemental Movie S1), and this was substantially increased in ROCK1 but not in ROCK2 KD cells. This result correlates well with the role of ROCK1 but not ROCK2 in promoting junctional tension, which retards intraepithelial cell movements.

Overall these data identify ROCK1 as a dominant architect of cadherin/actomyosin organization that establishes junctional tension, thus inhibiting epithelial motility.

ROCK1, but not ROCK2, supports RhoA signaling at the ZA

In addition to its role as an effector, we recently reported that ROCK can support junctional RhoA signaling itself. This involved a signaling feedback network in which ROCK phosphorylated Rnd3 to ultimately abrogate the junctional localization of the RhoA antagonist p190B RhoGAP (Priya *et al.*, 2015). Consistent with this, we found that inhibiting ROCK with Y-27632 destabilized the junctional pool of GFP-RhoA, reflected by an increase in GFP-RhoA mobile fraction measured by FRAP, and this was prevented by p190B KD (Figure 3, a–c). This provided further evidence that ROCK supports junctional Rho signaling by antagonizing p190B GAP. What effect the different ROCK proteins might have on this signaling network, however, was unknown.

To explore this question, we used endogenous Rho localization as a useful proxy to assess the integrity of the RhoA zone at the ZA (Ratheesh *et al.*, 2012). In control MCF-7 cells, RhoA exhibited prominent staining at the ZA, and this was substantially perturbed by ROCK1 siRNA without affecting total RhoA levels (Figure 3, d and e, and Supplemental Figure S3i). In contrast, depletion of ROCK2 had no effect on RhoA localization (Figure 3, d and e). To substantiate this notion, we then used a location biosensor for GTP-RhoA, GFP-AHPH (Piekny and Glotzer, 2008; Priya *et al.*, 2015; Yu *et al.*, 2016). This biosensor has been validated to faithfully recapitulate the dynamics of endogenous GTP-Rho (Priya *et al.*, 2015), and depletion of RhoA by small interfering RNA (siRNA) abolishes its junctional localization (Supplemental Figure S3, a–c). In control cells,

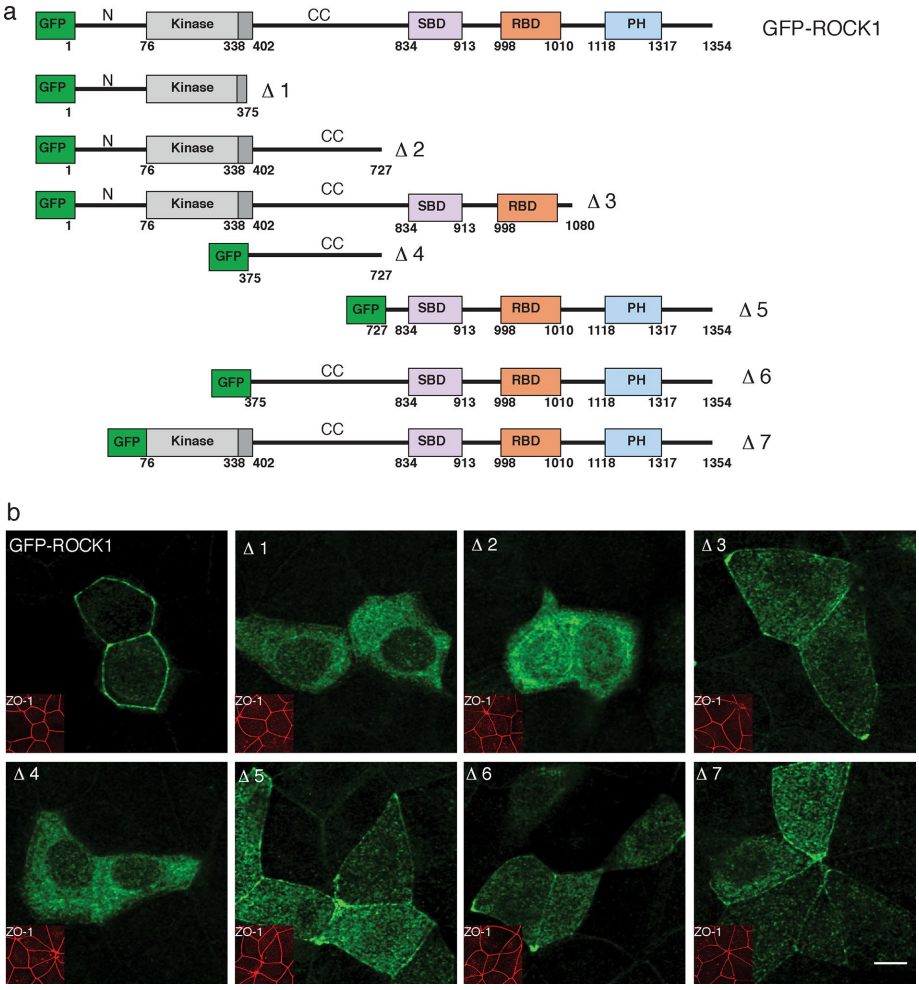

FIGURE 4: ROCK1 deletion-mutant analysis. (a) Domains of ROCK1 and the deletion constructs. (b) Representative confocal images of MCF-7 cells expressing various GFP-ROCK1 deletion constructs and immunostained for GFP and ZO-1.

GFP-AHPH showed a prominent junctional localization, and this was significantly reduced in ROCK1 siRNA cells (Figure 3, f and g). However, consistent with what we observed with endogenous RhoA, ROCK2 did not affect the AHPH signal at the ZA (Figure 3, f and g), implying that ROCK1 is predominantly responsible for supporting RhoA signaling at the ZA.

Of note, ROCK1 inhibition can stimulate Rac1 activity via Tiam1 and thereby potentially down-regulate RhoA by cross-talk (Tang *et al.*, 2012). However, we did not see any difference in Rac1 localization or activity when Rho kinase was inhibited or depleted (Figure 3, h and i, and Supplemental Figure S3, d–f). Alternatively, RhoA at epithelial cadherin junctions can be inactivated by either loss of the GEF ECT2 or gain of the GAP, p190B (Ratheesh *et al.*, 2012; Priya *et al.*, 2015). ROCK inhibition with Y27632 or its depletion by siRNA had no effect on ECT2 junctional localization (Figure 3, j and k, and Supplemental Figure S3, g and h), indicating that loss of this GEF could not explain the inhibition of RhoA signaling upon ROCK depletion. However, recruitment of p190B GAP to the ZA was significantly enhanced in the cells depleted of ROCK1, with no change in its expression levels (Figure 3, l and m, and Supplemental Figure S3i). Strikingly, ROCK2 KD had no significant effect on p190B GAP localization (Figure 3, l and m), explaining the selective loss of RhoA activity in ROCK1 KD cells. Overall these results establish that ROCK1, but not ROCK2, is required to support RhoA signaling at cadherin junctions and further suggest that it exerts this effect by antagonizing p190B recruitment (Priya *et al.*, 2015).

Mechanisms of ROCK1 localization at the ZA

Because ROCK1 appeared to be the major regulator of RhoA signaling and epithelial contractility at the ZA, we then sought to better understand how ROCK1 is localized at the ZA. We created GFP-tagged deletion mutants of ROCK1 and expressed them in MCF-7 cells. ROCK1 is structurally composed of a distinct N-terminal domain, a highly conserved serine-threonine kinase domain, a coiled-coil domain (CC), a RBD, a Shroom-binding domain (SBD), and a PH domain (Figure 4a). Wild-type GFP-ROCK1 showed a predominant localization at the apical junctions of cells (Figure 4, a and b). In contrast, the mutants Δ1, Δ2, and Δ4, which lack the RBD, SBD, and PH domains, were completely cytoplasmic (Figure 4, a and b), indicating that these three domains contribute to junctional localization of ROCK1. However, the mutant Δ5, comprising the RBD, SBD, and PH domains, was still poorly localized at the ZA (Figure 4, a and b), indicating that these previously identified domains were essential but not sufficient to confer junctional localization to ROCK1 (Simões Sde *et al.*, 2014), and possibly, as for ROCK2, deletion of the CC domain in this mutant compromises its scaffolding properties, thus attenuating its cortical association (Truebestein *et al.*, 2015).

This mutational analysis also indicates a previously unidentified role for the N-terminus in localizing ROCK1 at junctions, as the mutant Δ7, which lacks the first 76 amino acids, showed only weak cortical enrichment (Figure 4, a and b). The N-terminus of ROCK1 is very distinct from that of ROCK2 and is required for its dimerization, kinase activity, and Rnd3 regulation (Garg *et al.*, 2008). Thus it is possible that this region regulates ROCK1 binding to effectors required for its cortical localization. Overall these results suggest that multiple domains, including the N-terminus, RBD, SBD, and PH domains, cooperate to confer junctional localization upon ROCK1.

A potential explanation for the foregoing findings is that multiple mechanisms cooperate to promote junctional recruitment of ROCK1. These include GTP-RhoA, which binds directly to the RBD of ROCK1 and is required to relieve its autoinhibition (Amano *et al.*, 1996; Matsui *et al.*, 1996), as well as NMIIA, which we recently found to interact with ROCK (Priya *et al.*, 2015). Accordingly, we sought to further discriminate between these possibilities. One potential analytical difficulty, however, is that disruption of NMII also down-regulates RhoA signaling by disinhibiting the junctional recruitment of p190B (Priya *et al.*, 2015). To overcome this limitation, we delocalized NMIIA from junctions with blebbistatin (Smutny *et al.*, 2010) and also prevented the concomitant down-regulation of junctional RhoA with p190B GAP siRNA, a maneuver that sustains junctional GTP-RhoA (Priya *et al.*, 2015). Blebbistatin abrogated

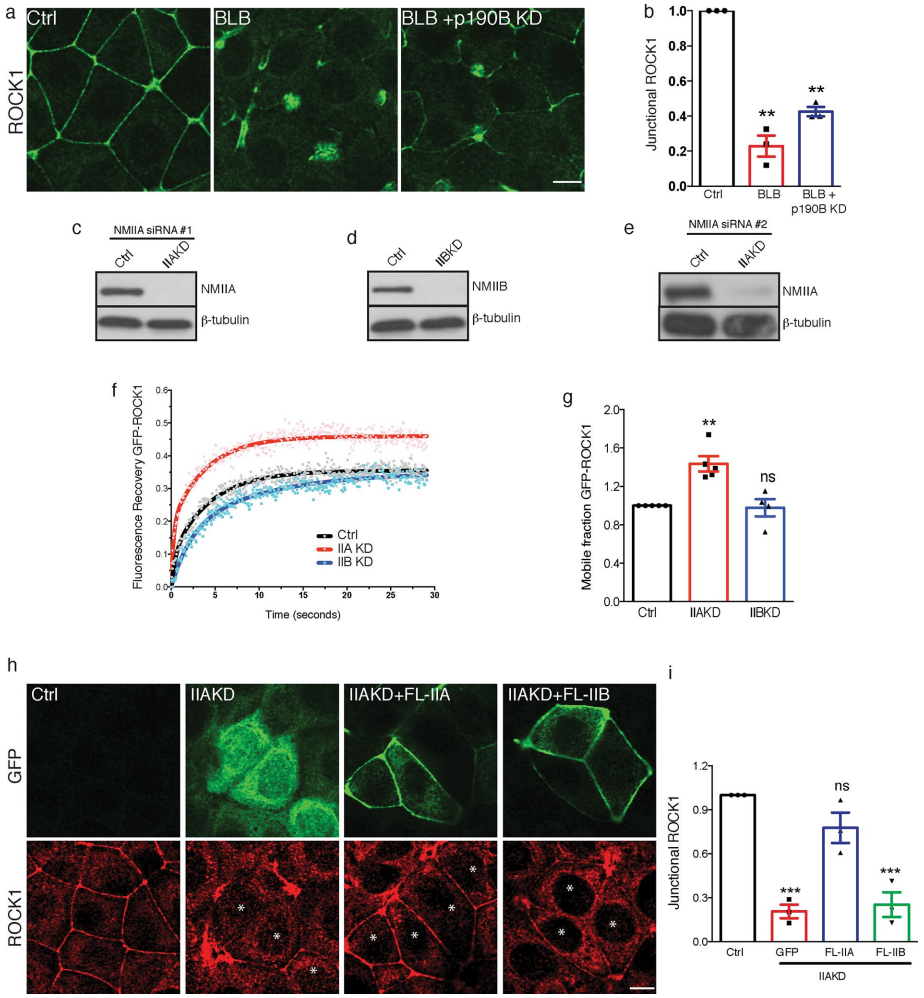

FIGURE 5: NMIIA contributes to ROCK1 localization at the ZA. (a, b) ROCK1 localization in ctrl or p190BKD MCF-7 cells treated with either dimethyl sulfoxide or blebbistatin; fluorescence intensity was quantified by line-scan analysis ($n = 3$). (c, d) Lysates from MCF-7 cells transduced with Ctrl, IIAKD, or IIBKD lentivirus immunoblotted for NMIIA, NMIIB, and β-tubulin, respectively. (e) Lysates from Ctrl or IIAKD (related to h and i) immunoblotted for NMIIA and β-tubulin. (f, g) FRAP of apical GFP-ROCK1 in Ctrl, IIAKD, and IIBKD MCF-7 cells. Mobile fraction values were calculated by fitting the recovery curves to a biexponential function in GraphPad Prism ($n = 4$). (h, i) ROCK1 localization in Ctrl or IIAKD MCF-7 cells transfected with GFP, GFP–NMIIA (FL IIA), or GFP–NMIIB (FL IIB); fluorescence intensity was quantified by line-scan analysis ($n = 3$).

ROCK1 cortical localization at the ZA, and this was not rescued by p190B siRNA (Figure 5, a and b), suggesting that RhoA signaling was not sufficient to stably localize ROCK1 at the ZA in the absence of an adequate pool of NMII. These findings reinforce the idea that NMII is one of the major determinants for ROCK1 junctional localization under these circumstances.

Therefore, to better evaluate the role of NMIIA and NMIIB in stabilizing ROCK1, we performed FRAP assays to test their effect on the junctional stability of ROCK1. Fluorescence recovery profiles indicate a significant increase in the mobile fractions of GFP-ROCK1 when NMIIA is depleted, whereas depletion of NMIIB has no effect (Figure 5, c, d, f, and g). This suggests that NMIIA is necessary to maintain a stable pool of ROCK1 at apical junctions. Consistent with this, we found that NMIIA depletion abolished the junctional localization of ROCK1, a phenotype that could be rescued by overexpressing NMIIA but not NMIIB in NMIIA KD cells (Figure 5, e, h, and i), reinforcing the selective contribution of NMIIA on ROCK1 localization.

In conclusion, our study identifies ROCK1 as the dominant ROCK that supports the ZA as a contractile junction in MCF-7 and Caco2 cells. NMIIA ensures the cortical stability of ROCK1, which in turn maintains the GTP-Rho zone, actomyosin organization, and junctional tension. Although ROCK-2 has been predicted to influence actin organization via cofilin (Shi *et al.*, 2013) or coronin1B (Rana and Worthylake, 2012) and tight junction assembly via cingulin (Terry *et al.*, 2011), we could not see any significant effect on actomyosin filament organization and tight junctions in cells depleted of ROCK2. Thus our findings contribute to the growing awareness that, despite having highly conserved enzymatic activities, ROCK1 and ROCK2 perform nonredundant functions. Future functional studies of Rho kinases should account for these biological differences and dissect them by incorporating selective inhibitors/reagents.

MATERIALS AND METHODS

Cell culture and transfections

MCF-7 cells were obtained from the American Type Culture Collection and cultured in DMEM (11995-073; Life Technologies, Grand Island, NY) supplemented with 10% fetal bovine serum (FBS), 1% nonessential amino acids, 1% L-glutamine, 100 U/ml penicillin, and 100 U/ml streptomycin. Cells were maintained with low-dose Plasmocin (Invitrogen, Grand Island, NY) and routinely examined for the presence of mycoplasma. For siRNA transfections, cells were cultured to 40–50% confluence and then transfected using RNAiMAX (Invitrogen) according to the manufacturer's recommendations. At 48–72 h posttransfection, cells were harvested for immunofluorescence assay or protein-expression analysis.

For transfection of plasmids, cells were cultured to 80–90% confluent, transfected using Lipofectamine 3000, and then fixed after 24 h for immunofluorescence assay. For live-cell experiments, cells were grown on 29-mm glass-bottom dishes (Shengyou Biotechnology) and imaged in clear Hanks' balanced salt solution (HBSS) supplemented with 5% FBS, 10 mM 4-(2-hydroxyethyl)-1-piperazineethanesulfonic acid (pH 7.4), and 5 mM $CaCl_2$.

siRNA and short hairpin RNA

ROCK1, p190B, and NMIIA were depleted using siRNAs designed via Invitrogen Block-iT RNAi designer against their untranslated regions. For all of these genes, two different siRNAs were ordered and then pooled to enhance the efficiency of knockdown. The control siRNAs used for these experiments were also combinations of two separate sequences. The sequences are as follows: p190B (NM_001030055.1_siRNA_5007 sense, GCAUGACUGGAGAGGUUUATT; and NM_001030055.1_siRNA_5063, sense, GCUGCUGCAUGCAACCUUATT), ROCK1 (NM_005406.2_stealth_866 sense,

CACCGCGGAGGAAGUUGGUUGAAAU; and NM_005406.2_stealth_904 sense, UGGUGCUGGUAAGAGGGCAUUGUCA), and NMIIA (5′-UAUAGCCAGGACCUGAACCUGGAUC-3′ and 5′-UUUAGAAUCAGGAGGGAGACAGCGG-3′).

ROCK2 and RhoA were depleted using commercially available SMARTpool siRNA (Dharmacon, Lafayette, CO), which is a premixed pool of four separate siRNAs. The sequences for ROCK2 siRNA are 5′-GCAGCAAUGGUAAGCGUAA-3′, 5′-GCAACUGGCUCGUUCAAUU-3′, 5′-GUAGAAACCUUCCCAAUUC-3′, and 5′-GCAAAUCUGUUAAUACUCG-3′, and those for RhoA siRNA are 5′-CGACAGCCCUGAUAGUUUA-3′, 5′-GACCAAAGAUGGAGUGAGA-3, 5′-GCAGAGAUAUGGCAAACAG-3, and 5′-GGAAUGAUGAGCACACAAG-3′.

NMIIA and NMIIB were depleted using lentiviral shRNA, as described previously (Smutny *et al.*, 2010).

Antibodies and inhibitors

Primary antibodies used in this study were mouse monoclonal antibody (mAb) HECD-1 against the ectodomain of E-cadherin (1:50; a gift from P. Wheelock, University of Nebraska, Omaha, NE; with the permission of M. Takeichi); rabbit polyclonal antibody (pAb) for nonmuscle myosin IIA heavy chain (1:1000; PRB-440P; Covance, Dedham, MA); rabbit pAb for nonmuscle myosin IIB heavy chain (1:1000; PRB-445P; Covance); mouse mAb (1:200; A-11120, clone 3E6; Molecular Probes/Invitrogen) against GFP; rabbit pAb (1:300; 61-7300; Invitrogen) and mouse mAb against human ZO-1 (1:300, \33-9100, clone ZO1-1A12; Invitrogen); mouse mAbs against RhoA (1:100; clone 26C4, sc418; Santa Cruz Biotechnology, Dallas, TX); rabbit pAb against Ect2 (1:50; 07-1364; Millipore, Billerica, MA); mouse mAbs against p190B (1:50, 611612, clone 54/P190-B; BD Biosciences, San Jose, CA); mouse mAb against β-tubulin (1:500, T4026, clone TUB 2.1; Sigma-Aldrich, St. Louis, MO); rabbit pAb against ROCK1 (1:300, AB134181; Abcam, Cambridge, MA); rabbit pAb to ROCK2 (1:100, AB71598; Abcam); mouse mAb against actin (1:100; MAB1501, clone number C4; Millipore); rat mAb E-cadherin (1:500, 13-1900, clone ECCD-2; Invitrogen); mouse mAb NMIIA (1:500, ab55456; Abcam), mouse mAb Rac1 (1:300, 05-389; Merck, Kenilworth, NJ); and mouse mAb pMRLC (1:100, 3675; Cell Signaling, Beverly, MA).

Secondary antibodies were species-specific antibodies conjugated with Alexa Fluor 488, 594, or 647 (1:500; Invitrogen) for immunofluorescence or horseradish peroxidase (1:5000; Bio-Rad Laboratories, Hercules, CA) for immunoblotting.

Cells were treated with blebbistatin to inhibit myosin (100 μM, 2 h; US1203390-5MG; Merck) or Y-27632 (30 μM, 1 h; Y0503; Sigma-Aldrich) to inhibit ROCK.

Plasmids

GFP–ROCK2 construct was generated by PCR-amplifying mouse ROCK2 using FLAG-tag mouse ROCK2 (a kind gift from M. Samuel, Centre for Cancer Biology, University of South Australia, Adelaide, Australia) as a template and cloned into pEGFP-C1 (Clontech) using *Eco*R1 and *Bam*H1 restriction sites. GFP-RhoA (12965), GFP-NMIIA (11347), and GFP-NMIIB (11348) were obtained from Addgene. GFP-ROCK1, E-cad–EGFP, and GFP-AHPH (used as a reporter for GTP-RhoA) have been described previously (Smutny *et al.*, 2011; Wu *et al.*, 2014; Priya *et al.*, 2015).

To generate GFP-ROCK1 deletion constructs, the coding region for ROCK1 (1–375 Δ1; 1–727 Δ2, 1–1080 Δ3, 375–727 Δ4, 727–1354 Δ5, 375–1354 Δ6, and 76–1354 Δ7) were amplified from GFP-ROCK1 and cloned into pEGFP-C1 using *Sac*1 and *Kpn*1 restriction sites.

Immunofluorescence microscopy

MCF-7 cells were fixed with ice-cold methanol for 5 min at –20°C or with freshly made 10% trichloroacetic acid (TCA; T0699-100ML; Sigma-Aldrich) on ice for 15 min or with 4% paraformaldehyde (PFA) in cytoskeleton stabilization buffer (10 mM 1,4-piperazinediethanesulfonic acid at pH 6.8, 100 mM KCl, 300 mM sucrose, 2 mM ethylene glycol tetraacetic acid, and 2 mM $MgCl_2$) on ice for 20 min. The cells fixed with TCA were subsequently washed three times with 30 mM glycine. To permeabilize TCA- and PFA-fixed cells, cells were incubated with 0.25% Triton X-100 for 5 min at room temperature and washed three times with phosphate-buffered saline (PBS). Confocal images were acquired using a Zeiss LSM-710 microscope or Zeiss LSM-510 META inverted microscope. For representation purposes, both control and test images were processed identically using ImageJ by applying a median filter of 0.5-1-pixel radius or by using the rolling-ball background subtraction function of ImageJ.

Quantification of fluorescence intensity at junctions

Fluorescence intensity at junctions was quantified using the plot profile function of ImageJ. Briefly, a line 10–20 μm in length was drawn orthogonal to the junctions with its center at the junctions. The plot profile function of ImageJ was then used to obtain the numerical values for the fluorescence intensity. Background correction was performed by subtracting a constant value from each of the intensity profiles and then fitted to Gaussian function using GraphPad Prism software. A nonlinear regression function was used to determine the peak values. For each experiment, a minimum of 40 contacts were analyzed per condition.

For the Rho biosensor experiment, the mean-gray values of GFP-AHPH junctional and cytoplasmic intensity were obtained using ImageJ, and their ratio was used for statistical analysis. This normalized ratio is referred to as junctional GTP-RhoA.

Although the GFP-AHPH biosensor does not distinguish between the RhoA/RhoB/RhoC proteins, crystal structure data and biochemical results show that the AH domain of anillin directly binds to GTP-RhoA (Piekny and Glotzer, 2008; Sun *et al.*, 2015). Further, using a series of mutants and pharmacological/genetic ablation studies, we validated that the junctional enrichment of AHPH strictly depends on its interaction with GTP-RhoA and thus recapitulates the endogenous localization of GTP-RhoA (Priya *et al.*, 2015; Supplemental Figure S3, b and c).

Laser ablation

To measure junctional tension in the steady state, MCF-7 cells were transduced with lentivirus encoding E-cadherin–EGFP (Wu *et al.*, 2014) to identify apical junctions. Then individual ROCK proteins were depleted using siRNA for 48–72 h. An LSM 510 Meta Zeiss confocal microscope equipped with a 37°C heating stage was used for the experiments, and images were acquired and analyzed as described previously (Wu *et al.*, 2014; Priya *et al.*, 2015).

Differences in recoil are useful indicators of contractile tension, as long as the viscous drag remains unchanged or is a minor contributor to the recoil (Sugimura *et al.*, 2016). To assess this, we modeled the mechanics of junctions as Kelvin–Voigt fibers and extracted the rate constants (*k* values), which reflect the ratio of elasticity to viscosity, from the recoil measurements (Michael *et al.*, 2016). We found no significant changes in *k* values in ROCK1 and ROCK2 KD cells compared with control cells (Supplemental Table S1), suggesting that the differences in the initial recoil velocities were principally due to changes in contractile tension.

FRAP

MCF-7 cells were transfected with GFP-NMIIA, GFP-RhoA, or GFP-ROCK1 and imaged in clear HBSS. Image acquisition and analysis was described previously (Priya and Gomez, 2013; Priya *et al.*, 2015).

Fluorescence resonance energy transfer

MCF-7 cells were transfected with a Raichu-Rac fluorescence resonance energy transfer (FRET) biosensor (Itoh *et al.*, 2002) and 24 h posttransfection were treated with either PBS or Y-27632 (30 μM, 1 h; Y0503; Sigma-Aldrich). For live-cell imaging, cells were incubated at 37°C in an LSM710 Zeiss confocal microscope equipped with a 63× oil immersion objective (Plan Apochromat 63×/1.4 numerical aperture [NA]; Zeiss). Images were acquired by sequential line acquisition. For the acceptor (A) channel, a 514-nm laser line was used for excitation, and emission was collected in the acceptor emission range (bandpass [BP] 530–590 nm). Donor and FRET channels were acquired using a 458-nm laser line, and emission was collected in the donor emission region (BP 470–490 nm) and the acceptor emission region (BP 530–590 nm, FRET). FRET measurements have been described previously (Ratheesh *et al.*, 2012).

Time-lapse imaging and nuclei tracking

Time-lapse live-cell imaging of MCF-7 cells stably expressing both Histone2b-GFP and a plasma membrane–targeted mCherry by fusing it to the C-terminal 14 amino acids of human K-Ras4B (mCherry-Mt) was performed on a Nikon Ti-E deconvolution microscope (40×/0.95 NA Plan Apo objectives) driven by NIS-Elements AR software (version 4.3; Nikon) equipped with a 37°C, 5% CO_2 chamber. Images were acquired every 3 min for 5 h on cells cultured in DMEM in the presence of 10% FBS. Movies of nuclei in movies were then tracked using the u-track software developed by the Danuser lab (lccb.hms.harvard.edu/software.html; Jaqaman *et al.*, 2008; Ng *et al.*, 2012), and mean square displacements for different time intervals were calculated using a custom-made MATLAB script, which is available upon request.

Statistics

Unless otherwise stated, data represent mean ± SEM, and *n* is the number of independent experiments. Precisely, *n* states the number of times each individual experiment was repeated at different times, thus accounting for the variability of the biological process.

For line-scan analysis, at least 40 contacts were analyzed per experiment, and for laser ablation and FRAP, a minimum of 20 contacts were analyzed per experiment, except for Rho-FRAP, for which 10–15 contacts were analyzed per experiment. Student's *t* test was used to compare two groups, and one-way analysis of variance (ANOVA) with corrections for multiple comparisons applied) was used to compare more than two groups. GraphPad Prism 6 was used to determine the *p* values and perform all statistical analyses. Student's *t* test was used for Figures 1i and 2, f and h, and Supplemental Figures S2g and S3e, f, and h. One-way ANOVA was used for Figures 1, f, k, and m, 2, k and m, 3, b, e, g, i, k, and m, and 5, g and i, and Supplemental Figures S1, e, h, and k, and S2, b and c.

NS, not significant. *$p < 0.05$; **$p < 0.01$; ***$p < 0.001$; ****$p < 0.0001$.

ACKNOWLEDGMENTS

We thank our laboratory colleagues for their unstinting support and advice during the course of this project, as well as our colleagues elsewhere for their kind gifts of reagents. This work was supported by grants and fellowships from the National Health and Medical Research Council of Australia (APP1037320, APP1067405, APP1044041), the Australian Research Council (DP150101367), and the Cancer Council of Queensland (APP1086857). G.A.G. was supported by the Kids Cancer Project of the Oncology Research Foundation and a University of Queensland Early Career Research Grant. R.P. was supported an ANZ Trustees PhD Scholarship in Medical Research. X.L. was supported by a University of Queensland (UQ)–China PhD scholarship and a UQ International (UQI) scholarship. J.L.T. is supported by an Equity Trustees PhD Scholarship in Medical Research and a UQ International (UQI) scholarship. K.D. was supported by a UQ International Scholarship.

REFERENCES

Amano M, Ito M, Kimura K, Fukata Y, Chihara K, Nakano T, Matsuura Y, Kaibuchi K (1996). Phosphorylation and activation of myosin by Rho-associated kinase (Rho-kinase). J Biol Chem 271, 20246–20249.

Amano M, Nakayama M, Kaibuchi K (2010). Rho-kinase/ROCK: a key regulator of the cytoskeleton and cell polarity. Cytoskeleton 67, 545–554.

Anderson SC, Stone C, Tkach L, SundarRaj N (2002). Rho and Rho-kinase (ROCK) signaling in adherens and gap junction assembly in corneal epithelium. Invest Ophthalmol Vis Sci 43, 978–986.

Andreeva A, Lee JY, Lohia M, Wu XJ, Macara IG, Lu XW (2014). PTK7-Src signaling at epithelial cell contacts mediates spatial organization of actomyosin and planar cell polarity. Dev Cell 29, 20–33.

Bishop AL, Hall A (2000). Rho GTPases and their effector proteins. Biochem J 348, 241–255.

Garg R, Riento K, Keep N, Morris JD, Ridley AJ (2008). N-terminus-mediated dimerization of ROCK-I is required for RhoE binding and actin reorganization. Biochem J 411, 407–414.

Gomez GA, McLachlan RW, Wu SK, Caldwell BJ, Moussa E, Verma S, Bastiani M, Priya R, Parton RG, Gaus K, *et al.* (2015). An RPTP alpha/Src family kinase/Rap1 signaling module recruits myosin IIB to support contractile tension at apical E-cadherin junctions. Mol Biol Cell 26, 1249–1262.

Hannemann S, Madrid R, Stastna J, Kitzing T, Gasteier J, Schonichen A, Bouchet J, Jimenez A, Geyer M, Grosse R, *et al.* (2008). The Diaphanous-related Formin FHOD1 associates with ROCK1 and promotes Src-dependent plasma membrane blebbing. J Biol Chem 283, 27891–27903.

Itoh RE, Kurokawa K, Ohba Y, Yoshizaki H, Mochizuki N, Matsuda M (2002). Activation of rac and cdc42 video imaged by fluorescent resonance energy transfer-based single-molecule probes in the membrane of living cells. Mol Cell Biol 22, 6582–6591.

Jacobs M, Hayakawa K, Swenson L, Bellon S, Fleming M, Taslimi P, Doran J (2006). The structure of dimeric ROCK I reveals the mechanism for ligand selectivity. J Biol Chem 281, 260–268.

Jaqaman K, Loerke D, Mettlen M, Kuwata H, Grinstein S, Schmid SL, Danuser G (2008). Robust single-particle tracking in live-cell time-lapse sequences. Nat Methods 5, 695–702.

Julian L, Olson MF (2014). Rho-associated coiled-coil containing kinases (ROCK): Structure, regulation, and functions. Small GTPases 5, e29846.

Kimura K, Ito M, Amano M, Chihara K, Fukata Y, Nakafuku M, Yamamori B, Feng J, Nakano T, Okawa K, *et al.* (1996). Regulation of myosin phosphatase by Rho and Rho-associated kinase (Rho-kinase). Science 273, 245–248.

Komander D, Garg R, Wan PT, Ridley AJ, Barford D (2008). Mechanism of multi-site phosphorylation from a ROCK-I:RhoE complex structure. EMBO J 27, 3175–3185.

Kumper S, Mardakheh FK, McCarthy A, Yeo M, Stamp GW, Paul A, Worboys J, Sadok A, Jorgensen C, Guichard S, Marshall CJ (2016). Rho-associated kinase (ROCK) function is essential for cell cycle progression, senescence and tumorigenesis. Elife 5, e12994.

Lock FE, Ryan KR, Poulter NS, Parsons M, Hotchin NA (2012). Differential regulation of adhesion complex turnover by ROCK1 and ROCK2. PLoS One 7, e31423.

Matsui T, Amano M, Yamamoto T, Chihara K, Nakafuku M, Ito M, Nakano T, Okawa K, Iwamatsu A, Kaibuchi K (1996). Rho-associated kinase, a novel serine threonine kinase, as a putative target for the small GTP binding protein Rho. EMBO J 15, 2208–2216.

Michael M, Meiring JC, Acharya BR, Matthews DR, Verma S, Han SP, Hill MM, Parton RG, Gomez GA, Yap AS (2016). Coronin 1B reorganizes the architecture of F-actin networks for contractility at steady-state and apoptotic adherens junctions. Dev Cell 37, 58–71.
Nakagawa O, Fujisawa K, Ishizaki T, Saito Y, Nakao K, Narumiya S (1996). ROCK-I and ROCK-II, two isoforms of Rho-associated coiled-coil forming protein serine/threonine kinase in mice. FEBS Lett 392, 189–193.
Newell-Litwa KA, Badoual M, Asmussen H, Patel H, Whitmore L, Horwitz AR (2015). ROCK1 and 2 differentially regulate actomyosin organization to drive cell and synaptic polarity. J Cell Biol 210, 225–242.
Ng MR, Besser A, Danuser G, Brugge JS (2012). Substrate stiffness regulates cadherin-dependent collective migration through myosin-II contractility. J Cell Biol 199, 545–563.
Piekny AJ, Glotzer M (2008). Anillin is a scaffold protein that links RhoA, actin, and myosin during cytokinesis. Curr Biol 18, 30–36.
Priya R, Gomez GA (2013). Measurement of junctional protein dynamics using fluorescence recovery after photobleaching (FRAP). Bio-Protocol 3, e937.
Priya R, Gomez GA, Budnar S, Verma S, Cox HL, Hamilton NA, Yap AS (2015). Feedback regulation through myosin II confers robustness on RhoA signalling at E-cadherin junctions. Nat Cell Biol 17, 1282–1293.
Priya R, Wee K, Budnar S, Gomez GA, Yap AS, Michael M (2016). Coronin 1B supports RhoA signaling at cell-cell junctions through Myosin II. Cell Cycle 15, 3033–3041.
Priya R, Yap AS, Gomez GA (2013). E-cadherin supports steady-state Rho signaling at the epithelial zonula adherens. Differentiation 86, 133–140.
Rana MK, Worthylake RA (2012). Novel mechanism for negatively regulating Rho-kinase (ROCK) signaling through coronin1B protein in neuregulin 1 (NRG-1)-induced tumor cell motility. J Biol Chem 287, 21836–21845.
Ratheesh A, Gomez GA, Priya R, Verma S, Kovacs EM, Jiang K, Brown NH, Akhmanova A, Stehbens SJ, Yap AS (2012). Centralspindlin and alpha-catenin regulate Rho signalling at the epithelial zonula adherens. Nat Cell Biol 14, 818–828.
Riento K, Ridley AJ (2003). Rocks: multifunctional kinases in cell behaviour. Nat Rev Mol Cell Biol 4, 446–456.
Riento K, Totty N, Villalonga P, Garg R, Guasch R, Ridley AJ (2005). RhoE function is regulated by ROCK I-mediated phosphorylation. EMBO J 24, 1170–1180.
Sandquist JC, Swenson KI, Demali KA, Burridge K, Means AR (2006). Rho kinase differentially regulates phosphorylation of nonmuscle myosin II isoforms A and B during cell rounding and migration. J Biol Chem 281, 35873–35883.
Shewan AM, Maddugoda M, Kraemer A, Stehbens SJ, Verma S, Kovacs EM, Yap AS (2005). Myosin 2 is a key Rho kinase target necessary for the local concentration of E-cadherin at cell-cell contacts. Mol Biol Cell 16, 4531–4542.
Shi J, Wu X, Surma M, Vemula S, Zhang L, Yang Y, Kapur R, Wei L (2013). Distinct roles for ROCK1 and ROCK2 in the regulation of cell detachment. Cell Death Dis 4, e483.
Simões Sde M, Mainieri A, Zallen JA (2014). Rho GTPase and Shroom direct planar polarized actomyosin contractility during convergent extension. J Cell Biol 204, 575–589.
Smith AL, Dohn MR, Brown MV, Reynolds AB (2012). Association of Rho-associated protein kinase 1 with E-cadherin complexes is mediated by p120-catenin. Mol Biol Cell 23, 99–110.
Smutny M, Cox HL, Leerberg JM, Kovacs EM, Conti MA, Ferguson C, Hamilton NA, Parton RG, Adelstein RS, Yap AS (2010). Myosin II isoforms identify distinct functional modules that support integrity of the epithelial zonula adherens. Nat Cell Biol 12, 696–702.
Smutny M, Wu SK, Gomez GA, Mangold S, Yap AS, Hamilton NA (2011). Multicomponent analysis of junctional movements regulated by myosin II isoforms at the epithelial zonula adherens. PLoS One 6, e22458.
Sugimura K, Lenne PF, Graner F (2016). Measuring forces and stresses in situ in living tissues. Development 143, 186–196.
Sun LF, Guan RF, Lee IJ, Liu YJ, Chen MR, Wang JW, Wu JQ, Chen ZC (2015). Mechanistic insights into the anchorage of the contractile ring by anillin and Mid1. Dev Cell 33, 413–426.
Tang AT, Campbell WB, Nithipatikom K (2012). ROCK1 feedback regulation of the upstream small GTPase RhoA. Cell Signal 24, 1375–1380.
Terry SJ, Zihni C, Elbediwy A, Vitiello E, Leefa Chong San IV, Balda MS, Matter K (2011). Spatially restricted activation of RhoA signalling at epithelial junctions by p114RhoGEF drives junction formation and morphogenesis. Nat Cell Biol 13, 159–166.
Truebestein L, Elsner DJ, Fuchs E, Leonard TA (2015). A molecular ruler regulates cytoskeletal remodelling by the Rho kinases. Nat Commun 6, 10029.
Wang Y, Zheng XR, Riddick N, Bryden M, Baur W, Zhang X, Surks HK (2009). ROCK isoform regulation of myosin phosphatase and contractility in vascular smooth muscle cells. Circ Res 104, 531–540.
Wu SK, Gomez GA, Michael M, Verma S, Cox HL, Lefevre JG, Parton RG, Hamilton NA, Neufeld Z, Yap AS (2014). Cortical F-actin stabilization generates apical-lateral patterns of junctional contractility that integrate cells into epithelia. Nat Cell Biol 16, 167–178.
Yoneda A, Multhaupt HA, Couchman JR (2005). The Rho kinases I and II regulate different aspects of myosin II activity. J Cell Biol 170, 443–453.
Yu HH, Dohn MR, Markham NO, Coffey RJ, Reynolds AB (2016). p120-catenin controls contractility along the vertical axis of epithelial lateral membranes. J Cell Sci 129, 80–94.